ARTICLE

Exploring Bonding Properties, Extraction and Separation Performance of Furan-based N,O-Hybrid Extractants for Am(III) and Eu(III)

Weiqing Dong, Lin Dai, An Yong Li*

School of Chemistry and Chemical Engineering, Southwest University, Chongqing 400715, China

(Dated: Received on December 25, 2024; Accepted on February 19, 2025)

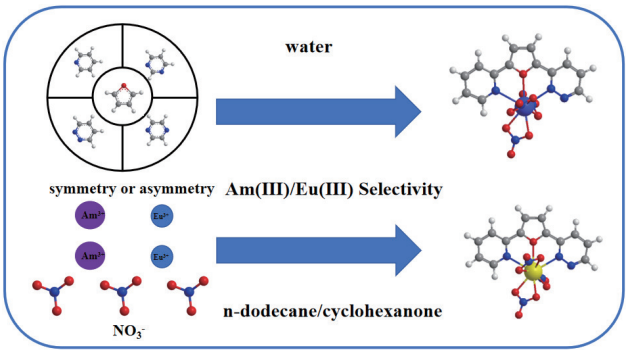

The Am(III) and Eu(III) in high-level liquid waste exhibit similar physicochemical properties, which makes their extraction and separation rather challenging. Ten symmetric and asymmetric furan-based N,O-hybrid extractants were constructed from the furan skeleton and the side chains of pyridine, pyridazine, pyrimidine and pyrazine. The density functional theory method was employed to evaluate the coordination structures and bonding properties of the ligands with the Am(III) and Eu(III) ions; the thermodynamic parameters of the two-phase extraction process were calculated to explore the extraction ability and separation performance of the ligands for the Am(III) and Eu(III) ions. The natural bond orbitals and QTAIM analyses show that there is a weak closed-shell interaction between Am(III), Eu(III) and the ligand, and the Am-ligand bonds have more covalent character than the Eu-ligand bonds since the Am-5f orbitals are more involved in bonding with the ligand than the Eu-4f orbitals. Thermodynamic analysis shows that the solvents cyclohexanone and *n*-dodecane of the organic phase have some impact on the extraction and separation, the ligand was more likely to bind with the metal in the cyclohexanone solvent, while some ligands have better separation effects in the n-dodecane solvent. In either solvents, the asymmetric extractant L^9 has the most excellent separation performance for the two metal ions, and the asymmetric ligands L^5 and L^8 also have good separation effect. This work contributes to a deeper understanding of the selectivity differences of similar furan-based flexible ligands and provides more abundant theoretical bases and insights for the design of new extractants required for the separation of Am(III) and Eu(III).

Key words: Bonding analysis, Lanthanide and actinide elements, Extraction and separation, Interaction

I. INTRODUCTION

Nuclear energy, as an important clean energy source, is gradually replacing fossil fuels because of its high energy density and its alignment with the concept of low-carbon economy. However, proper disposal of spent nuclear waste is the most critical factor in developing nuclear energy as a cost-effective and environmentally friendly energy source. The PUREX process, a classic method for nuclear fuel reprocessing, can extract most of plutonium and uranium in spent nuclear waste, while the high-level radioactive liquid waste after the PUREX

* Author to whom correspondence should be addressed. E-mail: ayli001@swu.edu.cn

process still contains minor actinide elements with high radioactivity and toxicity besides lanthanides and fission products [1–3]. The partition and transmutation strategy was put forward for the treatment of the high-level radioactive liquid wastes [4–6]. It selectively extracts minor actinide elements (U, Np, Pu, Am and Cm) from the high-level radioactive wastes, and then transmutes the long-lived actinides into short-lived or more stable nuclides, thus eliminating the potential impact of high radioactive nuclides on the environment [7, 8]. The lanthanides and actinides, such as Am(III) and Eu(III), have very similar physicochemical properties, such as similar oxidation states, ionic radii and similar hindrance factors, so their separation becomes a very challenging subject [9–11].

The separation of lanthanides and actinides has a long history, a large number of extractants have been developed to effectively extract and separate lanthanides and actinides, and a large number of theoretical calculations have also provided theoretical support for the effectiveness of these extractants. The ligands BTP [12, 13] and Terpy [14, 15] containing N-donor atoms have been shown to be able to effectively separate Am(III) from Eu(III). Since the separation process was carried out in an acidic aqueous phase, the protonation of the ligands can significantly affect the extraction of metal ions by ligands. Tributyl phosphate (TBP) can extract these two kinds of ions under specific conditions. It had a bipyridine skeleton connecting two isopropyl groups and phosphate substituents [16]. In this system, the cation coordination was significantly influenced by the nitrogen and oxygen atoms in the phosphoric acid bipyridine ligand. The existence of oxygen was of great significance. It could not only reduce the sensitivity of the extractant to acidity but also facilitate the separation of lanthanide and actinide elements at lower concentrations. The BTBP and its derivatives such as $CyMe_4$-BTBP (5,5,8,8-tetramethyl-5,6,7,8-tetrahydrobenzo-1,2,4-triazin-3-yl)-2,2′-bipyridine) were the reference molecules used in the development of the An(III)/Ln(III) separation process in Europe [4, 17, 18]. They have a good separation effect on lanthanide and actinide ions, and they have a tolerance to acidic environments and the ability to withstand the intense radiation generated by radiolysis during the separation process. Single crystal X-ray diffraction studies on different Ln(III)-BTBP 1:1 complexes clearly demonstrated the coordination mode of BTBP as a tetradentate chelating ligand [19]. A large number of solution studies have found that BTBP can extract An(III) and Ln(III) as 1:2 complexes [20]. In these complexes, the metal ions bond with both the extractant and the nitrate ions.

Bis-triazinyl pyridine is also a highly promising candidate extractant for the Am(III)/Eu(III) separation. It exhibits excellent separation performance and generate no secondary waste during its use [21]. The extraction process was carried out between the organic phase and the nitric acid aqueous phase containing the An(III)/Ln(III) mixture, the coordination of nitrate ions with metal ions is also critical for improving the ligands and the extraction process. Because the nitrate ions in the nitrate extraction system are prone to form inner-sphere complexes with lanthanide or actinide ions, this leads to competition during the coordination process and makes its coordination chemistry more complicated than that of other extraction systems. Information on the coordination of nitrate ions with metal ions can be provided by some experimental methods such as vibrational sideband spectroscopy (VSBS).

It was suggested that pre-organized ligands might possess better extraction performance compared to parent conformationally flexible ligands [22]. In this study, we construct ten symmetrical and asymmetrical flexible ligands by using 2,5-di(pyridin-2-yl)furan as a skeleton, and using pyridine, pyridazine, pyrimidine or pyrazine as the side chains, and we systematically investigated the coordination structures of these ligands with metal ions Am(III) and Eu(III) and their extraction and separation properties for Am(III) and Eu(III) ions. The molecular structures, electrostatic potential (ESP) and the frontier molecular orbitals of furan flexible ligands were calculated, and the bonding properties and the thermodynamic behaviors of the complexes formed by Am(III) and Eu(III) with furan-based ligands were evaluated. This study contributes to the understanding of the role of furan-based ligands in the separation of An(III)/Ln(III) and may be valuable for developing novel N,O-hybrid ligands for the separation of Am(III) and Eu(III).

II. COMPUTATIONAL DETAILS

The Gaussian 09 D01 program [23] was employed to perform all the calculations in this work. The geometric structures of the ligands as well as those of the complex-

DOI: 10.1063/1674-0068/cjcp2412162

es formed by the ligands with Am^{3+} and Eu^{3+} were optimized using density functional theory (DFT) method with the PBE0 functional (this method can reproduce the experimental geometries and ground state properties of f-element compounds and obtain relatively accurate results) in the gas phase and the organic phases of the *n*-dodecane and cyclohexanone solvents, and the conductor-like screening model (CPCM) [24, 25] was used for the solvent phase. The spin-orbit coupling has a minimal impact on the configurations of the system and the thermodynamic properties and so was ignored in this study [26, 27]. The 60 core electrons of Am^{3+} and the 28 core electrons of Eu^{3+} are replaced by the quasi-relativistic effective core potentials (RECP) [28, 29] and the corresponding ECP 60 MWB and ECP 28 MWB valence basis sets in the segmented contraction modes of Am and Eu were used. The remaining light elements such as C, H, O, and N were described using the 6-311G(d) basis set. For the optimized structures of the complexes, the vibrational frequencies were calculated. As all the optimized structures have no imaginary frequencies, they correspond to a local minimum of energy on the potential energy surface. It has been determined by experiments and theoretical calculations that the ground states of the Am^{3+} and Eu^{3+} complexes were the spin state with a spin multiplicity of 7.

The Multiwfn 3.8 [30] and NBO 5.0 [31, 32] programs were used to analyze the bonding properties of the complexes. In the gas phase, the ligands were optimized at the PBE0/6-311G(d) level and the HOMO and LUMO as well as the electrostatic potential (ESP) were calculated. For the the optimized configurations of the complexes, the quantum theory of atoms in molecules (QTAIM) parameters including electron density ρ, Laplacian $\nabla^2\rho$ of electron density and electron localization function (ELF), and the second-order stabilization energy were calculated to analyze the bonding properties of the complexes. With the combination of the Multiwfn wavefunction analysis program and the visual molecular dynamics (VMD) program [33], the independent response index (IRI) diagrams were plotted to analyze the bonding characteristics of these complexes. In addition, thermodynamic analysis of the extraction process was also carried out in the organic phases of n-dodecane and cyclohexanone, and the extraction ability and separation effect of the ligands for the Am(III) and Eu(III) were measured by using ΔG and $\Delta\Delta G$ of the extraction process, or the separation factor $SF_{Am/Eu}$ [34].

III. RESULTS AND DISCUSSION

A. Geometric and electronic structures of ligands

We selected furan as the skeleton and four kinds of N-heteraromatic rings, namely pyridine, pyridazine, pyrimidine and pyrazine as side chains to construct 10 symmetric and asymmetric ligands. The interaction between trivalent f-block metal ions and organic bases is essentially mainly ionic in nature. The electrostatic potential (ESP) of molecules is a powerful tool for evaluating ionic interaction. The ESP diagrams of the ligands can be used to judge the affinity of the ligands for metal ions as well as their main binding sites. The ten constructed ligands were geometrically optimized at the PBE0/6-311G(d) level in gas phase, and their ESP diagrams are shown in FIG. 1, where red indicates a negative ESP and blue indicates a positive ESP.

It can be seen that the position with the most negative ESP is located in the cavity formed by the N and O atoms, thus this region is the chemical active center. The O atom on the furan and the two N atoms on the two side chains are the donor atoms coordinated with the metal ion. The maximum negative ESP value of these ligands changes obviously with the change of the side chain. For the four ligands (L^1, L^2, L^3, L^4) with two symmetrical side chains, the L^1 and L^2 with the side chains of pyridine and pyridazine, respectively, have much larger negative ESP values than the ligands L^3 and L^4 with the side chains of pyrimidine and pyrazine, respectively. Among the six asymmetric ligands, the ligand L^5 with the side chains of pyridine and pyridazine has the largest negative ESP value, and the ligand L^{10} with the side chains of pyrimidine and pyrazine has the smallest negative ESP value. Therefore, the ESP analysis shows that pyridine and pyridazine as side chains are more favorable for coordination with metal ions than pyrimidine and pyrazine as side chains.

The frontier MOs HOMO and LUMO have some value for analyzing the chemical, optical, and electrical properties of molecules. FIG. 2 shows the HOMO–LUMO diagrams and their energy levels calculated at the PBE0/6-311G(d) level in the gas phase. A smaller HOMO–LUMO energy gap usually corresponds to higher chemical reactivity. It can be seen that the HOMOs of these ligands are π bonding orbitals mainly located on the furan skeleton, while the LUMOs are π antibonding

DOI: 10.1063/1674-0068/cjcp2412162

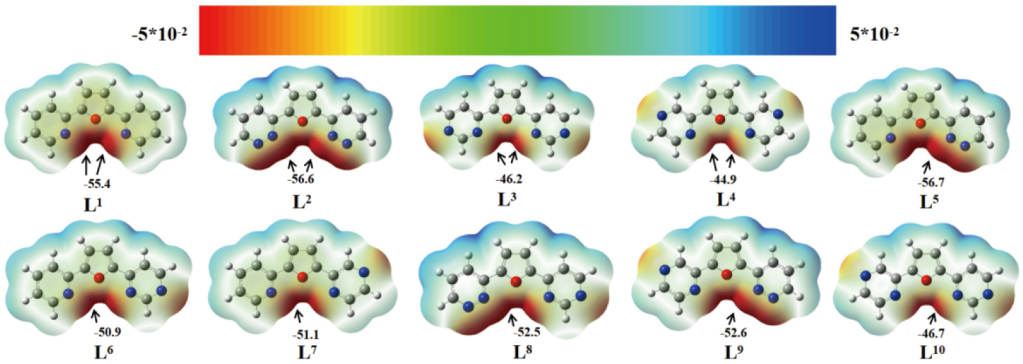

FIG. 1 ESP diagrams of the ligands calculated at the PBE0/6-311G(d) theoretical level (isosurface of electron density: 0.001 e/Å³).

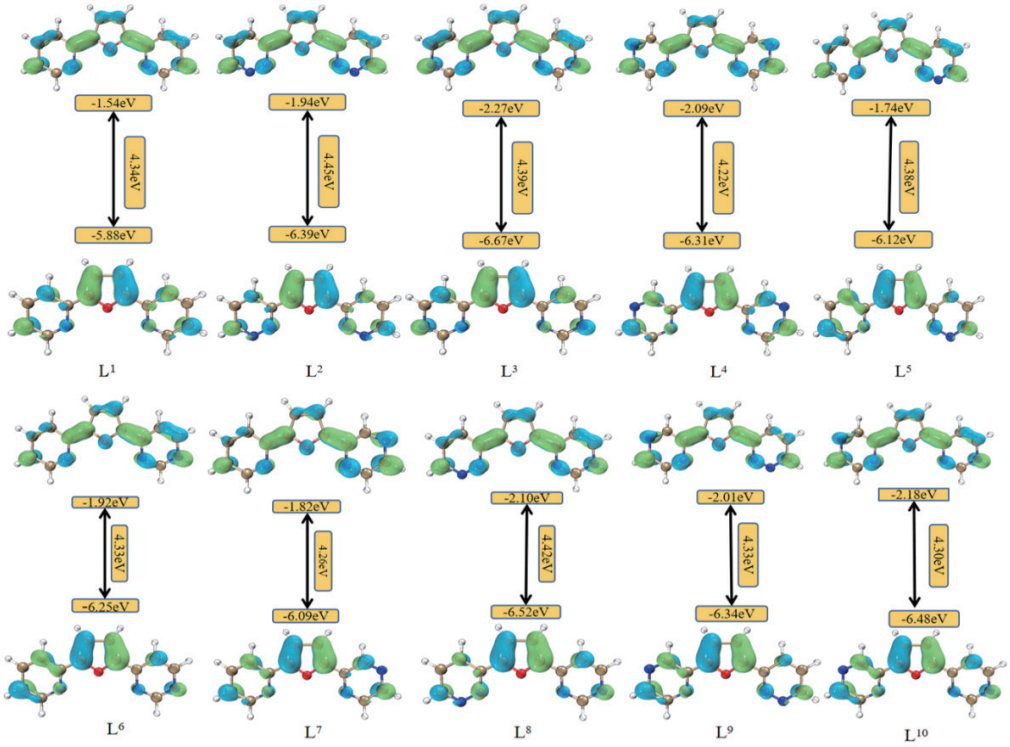

FIG. 2 HOMO–LUMO diagrams of the ligands calculated by the PBE0/6-311G(d) method.

orbitals located on both the skeleton and side chains. The energy gaps range from 4.22 eV to 4.45 eV, and ligands L^2 and L^8 have the largestest gaps (4.45 and 4.42 eV), while ligands L^4 and L^7 have the least gaps (4.22 and 4.26 eV). The side chains obviously influence the energy levels and energy gaps, but there is no obvious regularity.

We calculated the natural atomic charges on the donor-N/O atoms of the ligands using the PBE0/6-311G(d) method in the gas phase, the cyclohexanone organic phase, and the n-dodecane organic phase respectively. The average natural atomic charges are shown in Table I, Tables S1, S2 (Supplementary mate-

TABLE I Average natural charges (a.u.) of N and O atoms at the binding sites of ten ligands in the gas phase calculated by the PBE0/6-311G(d) method.

Ligand	O_{oxole}	$N_{pyridine}$	$N_{pyridazine}$	$N_{pyrimidine}$	$N_{pyrazine}$
L^1	−0.40	−0.44			
L^2	−0.39		−0.21		
L^3	−0.40			−0.47	
L^4	−0.39				−0.41
L^5	−0.39	−0.44	−0.21		
L^6	−0.40	−0.44		−0.47	
L^7	−0.40	−0.44			−0.41
L^8	−0.39		−0.21	−0.47	
L^9	−0.40		−0.21		−0.40
L^{10}	−0.40			−0.47	−0.40

DOI: 10.1063/1674-0068/cjcp2412162

TABLE II The calculated free energy (ΔG_O and ΔG_N, kcal/mol) at the O and N binding sites of the ligands calculated at the PBE0/6-311G(d) theoretical level for the reactions (R1) $L+H^+=LH^+$ (gas phase), (R2) $L+H_3O^+=LH^++H_2O$ (gas phase), and (R3) $L+H_3O^+=LH^++H_2O$ (aqueous phase).

Ligand	R1		R2		R3	
	ΔG_O	ΔG_N	ΔG_O	ΔG_N	ΔG_O	ΔG_N
L^1	−191.65	−231.17	−28.60	−68.78	−32.69	−32.30
L^2	−184.08	−217.92	−21.02	−55.52	−22.38	−29.50
L^3	−178.894	−221.72	−15.84	−59.32	−26.08	−25.80
L^4	−179.45	−210.25	−16.39	−47.85	−27.79	−24.33
L^5	−229.04	−229.05, −231.50	−65.98	−65.99, −68.45	−31.40	−31.37, −30.60
L^6	−226.38	−226.39, −224.53	−63.33	−63.33, −61.48	−30.83	−30.83, −27.43
L^7	−227.50	−227.50, −221.57	−64.44	−64.44, −58.51	−31.42	−31.42, −25.30
L^8	−226.40	−226.40, −222.20	−63.35	−63.35, −59.14	−16.10	−28.87, −26.37
L^9	−227.73	−227.73, −219.18	−64.67	−64.67, −56.13	−29.58	−29.58, −24.23
L^{10}	−220.78	−220.75, −216.45	−57.69	−57.69, −53.39	−17.05	−26.47, −23.61

rials, SM), respectively. It can be seen that the natural atomic charge of the N and O donor atoms are mainly determined by the aromatic ring where they are located, the influence in the other parts and the solvent effect on their natural atomic charges is relatively small. In the gas phase and different solvent phases, the difference of the natural atomic charges is relatively small, and the regularity is consistent. The charge in the solvent phase is slightly lower than the charge in the gas phase. In the gas phase, the charge on the O atom of furan is about −0.40 a.u. The N atoms of pyridine, pyrimidine and pyrazine have a little more negative charges, being −0.44 a.u., −0.47 a.u., and −0.41 a.u., respectively, while the N donor atom of pyridazine has a much smaller negative charge, only −0.20 a.u., which may be due to the competitive effect between the two adjacent N atoms greatly reducing the charge on the donor atom. It is notable that the N atoms of pyrimidine have the most negative charge among all these N-containing heterocyclic compounds.

During the process of metal ion extraction and separation between the organic phase and the acidic aqueous phase, the ligands are prone to undergo protonation, which affects the extraction effect of ligands on metal ions. We evaluated the proton affinity (PA) of the ligands through three reactions: (R1) $L+H^+=LH^+$ (gas), (R2) $L+H_3O^+=LH^++H_2O$ (gas), and (R3) $L+H_3O^+=LH^++H_2O$ (aqueous). The calculated free energies ΔG of the protonation reactions are shown in Table II. In the gas phase, the free energy of the ligand directly binding to the proton H^+ is much greater than that of extracting the proton H^+ from the hydronium ion H_3O^+. For the protonation reaction $L+H_3O^+=LH^++H_2O$, the solvation effect reduces the value of the free energy ΔG by 40–50 kcal/mol (except for the ΔG_O of L^1, L^2, L^3, L^4). It is notable that the ΔG_O is close to ΔG_N in the aqueous phase, and ΔG_N decreases in the order of pyridine, pyridazine, pyrimidine and pyrazine, but the free energies ΔG_N of protonation are very similar for different N heterocyclic rings, so their protonation trends are very close.

B. Structures of $ML(NO_3)_3$ complexes

We investigate the geometrical structures of the complexes formed by the Am(III)/Eu(III) metal ions with the ligands. It has been shown by previous studies that the Am(III)/Eu(III) ions can form 8–10 coordinated complexes with ligands in solution. The studied ligands are tridentate, and the nitrate ion also participates in the coordination with the metal ion. We consider the 1:1 (M:L), neutral 9-coordination complex $ML(NO_3)_3$, which is usually the metal-ligand complex formed during the actual extraction process. The geometrical structures of the complexes were optimized using the PBE0/6-311G(d)-RECP method in the gas phase, the cyclohexanone organic phase, and the n-dodecane organic phase, respectively. The geometries of the complexes are shown in FIG. 3, and the bond lengths of M–O(L), M–N(L) as well as the average bond length of M–O(NO_3) are listed in Table III, Tables S3, S4 (SM).

The calculated data in the gas phase show that the M–O(NO_3) bond is the shortest among the M–O and M–N bonds, ranging from 2.405 to 2.474 Å, and the

DOI: 10.1063/1674-0068/cjcp2412162

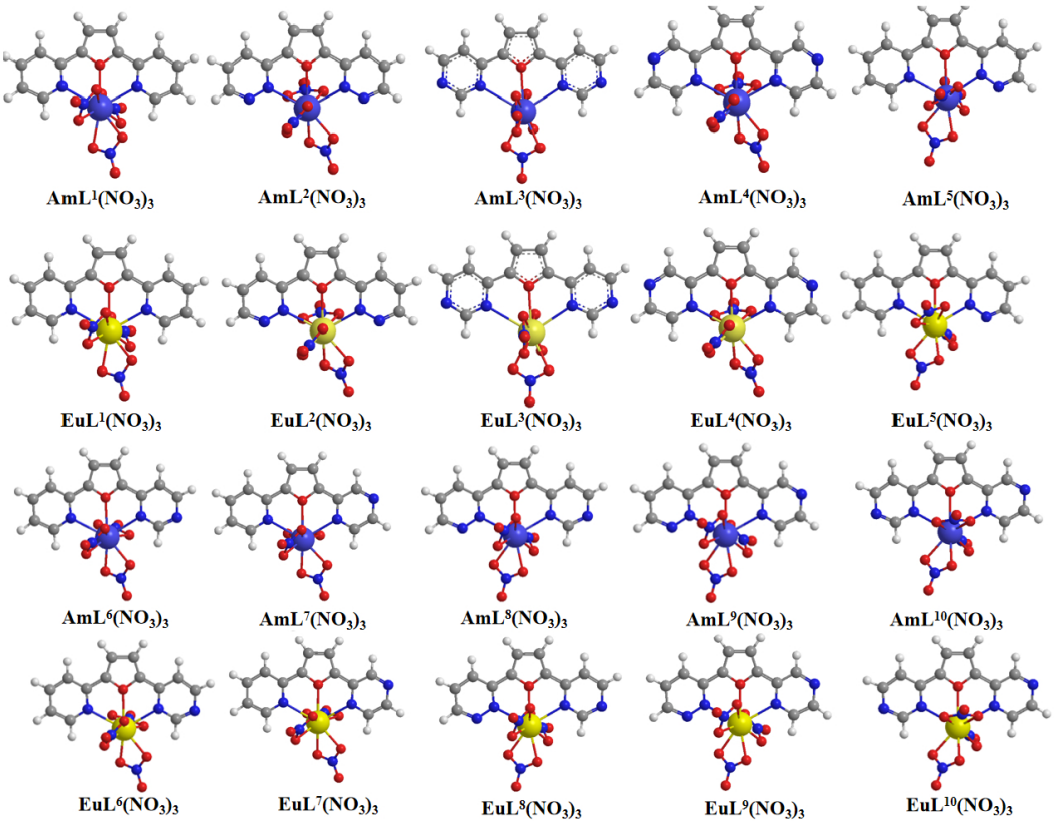

FIG. 3 Structures of $ML(NO_3)_3$ (M=Am, Eu) complexes optimized by the PBE0/6-311G(d)-RECP method. Herein, H, C, O, N, Am, and Eu are represented by white, gray, red, blue, purple, and yellow colors respectively.

TABLE III Bond lengths (Å) of M–O(L), M–N and the average bond length of M–O(NO_3) for $ML(NO_3)_3$ (M=Am, Eu) complexes in the gas phase at the PBE0/6-311G(d)-RECP theoretical level. Here the four N donor atoms are N1(pyridine), N2(pyridazine), N3(pyrimidine), and N4(pyrazine), respectively.

Complex (gas)	Bond length					
	M–O(L)	M–N1	M–N2	M–N3	M–N4	M–O(NO_3)
$ML^1(NO_3)_3$	2.569/2.538	2.668/2.642				2.447/2.405
$ML^2(NO_3)_3$	2.677/2.623		2.648/2.647			2.442/2.439
$ML^3(NO_3)_3$	2.636/2.580			2.667/2.646		2.474/2.453
$ML^4(NO_3)_3$	2.589/2.562				2.679/2.644	2.430/2.417
$ML^5(NO_3)_3$	2.652/2.591	2.708/2.666	2.629/2.591			2.456/2.407
$ML^6(NO_3)_3$	2.592/2.555	2.673/2.653		2.698/2.669		2.442/2.457
$ML^7(NO_3)_3$	2.590/2.546	2.678/2.659			2.681/2.665	2.448/2.435
$ML^8(NO_3)_3$	2.637/2.595		2.649/2.646	2.707/2.668		2.437/2.423
$ML^9(NO_3)_3$	2.637/2.611		2.639/2.623		2.711/2.702	2.441/2.403
$ML^{10}(NO_3)_3$	2.603/2.566			2.686/2.724	2.685/2.637	2.439/2.415

Note: Values before and after symboles "/" represent the results of the Am(III) and Eu(III) complexes, respectively.

M–O(L) bonds are generally shorter than the M–N bonds. Among the M–N bonds of all the complexes, the M–N2(pyridazine) bond length is generally quite shorter than the M–N1(pyridine), M–N3(pyrimidine), and M–N4(pyrazine) bonds lengths by at least 0.02 Å (an exception is that for the symmetrical ligands L^1, L^2, L^3, L^4, the Eu–N2 bond is a little longer than the Eu–L1, Eu–L3 and Eu–L4 bonds.). This means that due to the strengthening of the *ortho*-N atom, pyridazine has a stronger coordination bonding ability with metal ions than pyridine, pyrimidine, and pyrazine, consistent with the ESP analysis. This explains why the extractants used in the actual extraction process are all built with pyridazine as the side chain. The Am–O and

DOI: 10.1063/1674-0068/cjcp2412162

TABLE IV Average Wiberg bond indices (WBIs) of M–O(L), M–N, and M–O(NO_3) bonds in $ML(NO_3)_3$ (M=Am, Eu) complexes calculated at the PBE0/6-311G(d)-RECP theoretical level in the gas phase. Here the four N donor atoms are N1(pyridine), N2(pyridazine), N3(pyrimidine), and N4(pyrazine), respectively.

Complex	Average Wiberg bond indices					
	M–O(L)	M–N1	M–N2	M–N3	M–N4	M–O(NO_3)
$ML^1(NO_3)_3$	0.044/0.023	0.090/0.068				0.139/0.118
$ML^2(NO_3)_3$	0.031/0.027		0.087/0.063			0.143/0.107
$ML^3(NO_3)_3$	0.044/0.044			0.080/0.068		0.135/0.100
$ML^4(NO_3)_3$	0.048/0.034				0.092/0.054	0.146/0.098
$ML^5(NO_3)_3$	0.042/0.032	0.082/0.073	0.073/0.072			0.162/0.128
$ML^6(NO_3)_3$	0.023/0.033	0.082/0.070		0.081/0.061		0.136/0.126
$ML^7(NO_3)_3$	0.039/0.034	0.088/0.069			0.073/0.066	0.141/0.111
$ML^8(NO_3)_3$	0.039/0.030		0.075/0.064	0.084/0.065		0.145/0.117
$ML^9(NO_3)_3$	0.035/0.031		0.075/0.059		0.084/0.067	0.135/0.109
$ML^{10}(NO_3)_3$	0.038/0.031			0.069/0.053	0.086/0.073	0.135/0.117

Note: Values before and after symbols "/" represent the results of the Am(III) and Eu(III) complexes, respectively.

Am–N bonds are generally longer than the corresponding Eu–O and Eu–N bonds, respectively, while the difference between them is always smaller than the difference between the ionic radius of Am(III) (1.070 Å) and Eu(III) (0.995 Å) ions, thus the Am–ligand bonds are always stronger than the corresponding Eu–ligand bonds, which implies that the ligands can separate the Am(III) and Eu(III) ions. The calculated data in the organic phases of cyclohexanone and n-dodecane show the same regularity as the gas phase data.

C. Bonding properties of $ML(NO_3)_3$ complexes

The extraction and separation properties of the metal ions Am(III) and Eu(III) by the ligands can generally be understood through the bonding properties between the metal ions and the ligands. Several kinds of parameters can be used to analyze bonding properties, including Wiberg bond indices (WBIs), QTAIM parameters, density of states analysis (DOS), the second-order stabilization energy and the donor-acceptor interaction, and so on. The WBI values of the M–O(L), M–N and M–O(NO_3) bonds were calculated at the PBE0/6-311G(d)-RECP and are listed in Table IV. The M–O(NO_3) bonds have the largest WBI values among all these metal-ligand bonds, consistent with the bond lengths; while the M–O(L) bonds have much smaller WBI values than the M–N bonds, which is inconsistent with the bond length relationship between them. Among the M–N bonds, the M–N2 bond has the shortest bond length while it does not have the largest WBI values. These facts show that the WBI value is not suitable for measuring the strength of the key in some cases. The WBI values may be used to measure the covalent character of chemical bonds. Among these metal–ligand bonds, the M–O(NO_3) bonds have the strongest covalent character, and the M–N bond has a stronger covalent character than the M–O(L) bond. The Am–ligand bonds have larger WBI values than the corresponding Eu–ligands, which is consistent with their bond length relationship and implies that the Am–ligand bonds are more covalent than the corresponding Eu–ligand bonds. This provides some theoretical basis for the separation of Am(III) and Eu(III) by the ligands.

Topological analysis of electron density was further carried out based on Bader's theory of atoms in molecules with the Multiwfn software to investigate the nature of the metal-ligand bonds in all the complexes [35]. The QTAIM parameters, including electron density ρ, the Laplacian of electron density $\nabla^2\rho$ and the local electron energy density $H(r)$ at the BCPs of the M–O(L), M–N and M–O(NO_3) bonds in the complexes $ML(NO_3)_3$, were calculated at the PBE0/6-311G(d)-RECP level and the results are listed in Table S5 (SM). It can be seen that for all these M–O and M–N bonds, the electron density ρ at the BCP is less than 0.10 a.u., in the range of 0.01–0.06 a.u., and the electron density Laplacian $\nabla^2\rho$ is greater than zero, which implies that all these metal-ligand bonds are typical closed shell interactions. The local electron energy density $H(r)$ at the BCPs of the Am–N and Am–O(NO_3) bonds and the Eu–O(NO_3) bond is negative, indicating that these bonds have some covalent character; on the contrary, the $H(r)$ at the BCPs of the Am–O(L) and Eu–O(L)

DOI: 10.1063/1674-0068/cjcp2412162

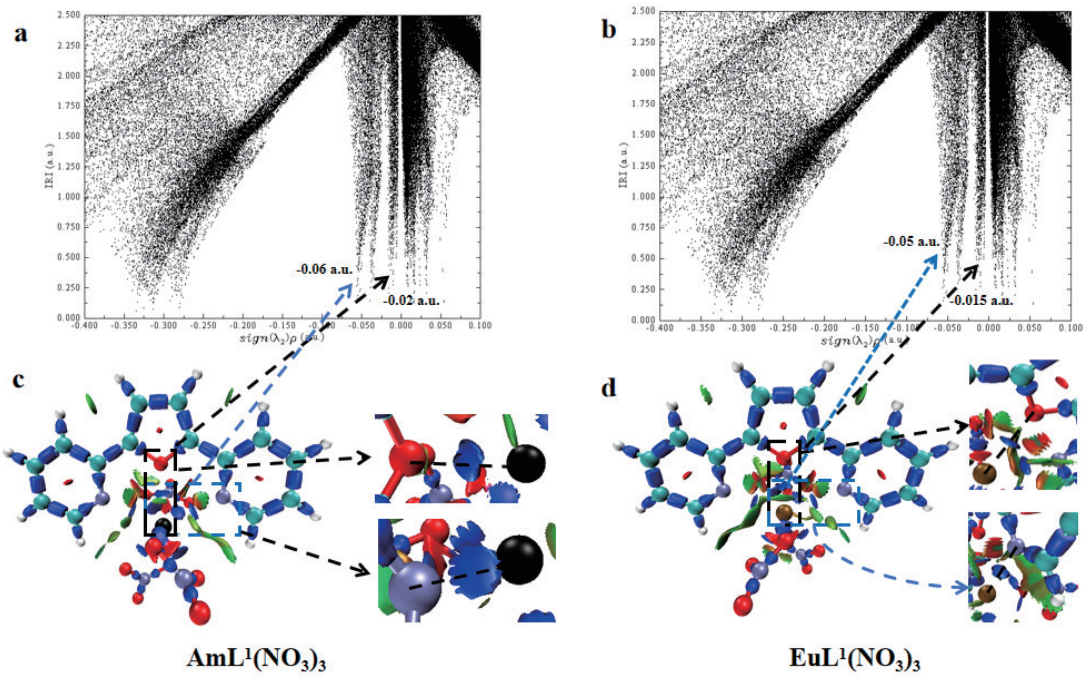

FIG. 4 (a) and (b) The scatter plots of the complexes $AmL^1(NO_3)_3$ and $EuL^1(NO_3)_3$ calculated at the PBE0/6-311G(d)-RECP level; (c) and (d) the partially colored IRI maps of $AmL^1(NO_3)_3$ and $EuL^1(NO_3)_3$.

bonds is positive, which means that these bonds are mainly ionic interactions. In these complexes, the M–O(NO_3) bond has the largest electron density ρ among all the metal-ligand bonds, and the M–N bonds also have a larger electron density than the M–O(L) bond. These indicate that the M–N bonds have greater covalent character than the M–O(L) bond, consistent with the WBI results. In addition, the Am–ligand bonds have a larger BCP electron density and a more negative $H(r)$ than the corresponding Eu–ligand bonds, thus the former has more covalent character than the latter, also consistent with the WBI analysis.

We further explored the bonding characteristics and interaction mechanisms between the metal ions Am^{3+}/Eu^{3+} and the ligands using the newly developed real-space function — the interaction region indicator (IRI). The IRI function is defined as $IRI(r)=|\nabla\rho(r)|/[\rho(r)]^a$, where '$a$' is a user-defined parameter, and according to previous reports, the optimal effect can be achieved when 'a' is set to 1.1. The IRI function can clearly present all types of interactions in graphics through isosurfaces and is an effective method to describe and reveal weak interaction regions as well as chemical bonds. The sign(λ_2)ρ function is projected onto the IRI isosurfaces in different colors to distinguish the intensity and characteristics of different regions. The scatter plots of $AmL^1(NO_3)_3$ and $EuL^1(NO_3)_3$ are presented in FIG. 4 (a) and (b), and the partially colored IRI maps of $AmL^1(NO_3)_3$ and $EuL^1(NO_3)_3$ are shown in FIG. 4 (c) and (d) which display the isosurface maps of the complexes with IRI = 1.0. In the scatter plots FIG. 4 (a) and (b), there are three spike points between −0.10 a.u. and 0 a.u., which correspond to the interactions between the two N–M bonds and O–M bond. In FIG. 4 (c) and (d), there are some blue regions between the central metal ions Eu^{3+}, Am^{3+} and the ligand O and N donors, which intuitively demonstrate the weak bonding interaction between the metals and the ligands.

The bonding characteristics of the metal–ligand interaction can be further analyzed by means of the donor–acceptor interaction between the metal ions and the ligands. The second-order stabilization energy ($\Delta E_{ij}^{(2)}$) of α-spin and β-spin between the donor natural bond orbitals (NBOs) of the ligand and the acceptor NBO of the metal ion in the complexes as well as the composition of the metal acceptor NBOs were calculated at the PBE0/6-311G(d)-RECP level in the gas-phase environment and are shown in Table V and Table S6 (SM). The second-order perturbation stabilization energy between the donor NBO and the acceptor NBO can be used to measure the strength and covalency of the bond interaction. The following conclusions can be drawn from the analysis of Table V and Table S6 (SM).

DOI: 10.1063/1674-0068/cjcp2412162

TABLE V The second-order stabilization energy ($\Delta E_{ij}^{(2)}$, in kcal/mol) of α spin between donor NBO(i) and acceptor NBO(j) in complex $ML(NO_3)_3$ and the composition of metal acceptor NBOs calculated at the level of PBE0/6-311G(d)-RECP.

Complex	NBO(i) → NBO(j)	$\Delta E_{ij}^{(2)}$	$\sum\Delta E_{ij}^{(2)}$	Character of the acceptor metal orbitals
$AmL^1(NO_3)_3$	LP(N/O)→LP*(Am^{3+})7s LP(N/O)→LP*(Am^{3+})5f	13.71 4.37	18.08	s(98.54%)p(0.06%)d (0.26%)f(1.13%) s(0.74%)p(0.17%)d(18.72%)f(80.36%)
$EuL^1(NO_3)_3$	LP(N/O)→LP*(Eu^{3+})6s LP(N/O)→LP*(Eu^{3+})4f	14.70 1.28	15.98	s(99.50%)p(0.06%)d(0.29%)f(0.13%) s(0.11%)p(0.03%)d(12.61%)f(87.23%)
$AmL^2(NO_3)_3$	LP(N/O)→LP*(Am^{3+})7s LP(N/O)→LP*(Am^{3+})5f	14.69 1.14	15.83	s(97.69%)p(0.05%)d(0.40%)f(1.86%) s(1.53%)p(0.28%)d(3.38%)f(94.81%)
$EuL^2(NO_3)_3$	LP(N/O)→LP*(Eu^{3+})6s LP(N/O)→LP*(Eu^{3+})4f	13.01 0.54	13.55	s(99.33%)p(0.05%)d(0.50%)f(0.10%) s(0.06%)p(0.05%)d(15.18%)f(84.68%)
$AmL^3(NO_3)_3$	LP(N/O)→LP*(Am^{3+})7s LP(N/O)→LP*(Am^{3+})5f	15.66 1.13	16.79	s(99.49%)p(0.05%)d(0.35%)f(0.10%) s(0.01%)p(0.07%)d(6.19%)f(93.72%)
$EuL^3(NO_3)_3$	LP(N/O)→LP*(Eu^{3+})6s LP(N/O)→LP*(Eu^{3+})4f	15.01 0.68	15.69	s(95.99%)p(0.04%)d(0.39%)f(3.55%) s(3.12%)p(0.11%)d(19.56%)f(77.13%)
$AmL^4(NO_3)_3$	LP(N/O)→LP*(Am^{3+})7s LP(N/O)→LP*(Am^{3+})5f	16.29 2.07	18.36	s(96.63%)p(0.06%)d(0.22%)f(3.10%) s(2.35%)p(0.22%)d(17.62%)f(79.81%)
$EuL^4(NO_3)_3$	LP(N/O)→LP*(Eu^{3+})6s LP(N/O)→LP*(Eu^{3+})4f	13.89 0.48	14.37	s(98.55%)p(0.06%)d(0.29%)f(1.08%) s(0.82%)p(0.09%)d(31.03%)f(67.97%)
$AmL^5(NO_3)_3$	LP(N/O)→LP*(Am^{3+})7s LP(N/O)→LP*(Am^{3+})5f	15.19 1.04	16.23	s(98.56%)p(0.04%)d(0.43%)f(0.97%) s(0.80%)p(0.05%)d(10.01%)f(89.14%)
$EuL^5(NO_3)_3$	LP(N/O)→LP*(Eu^{3+})6s LP(N/O)→LP*(Eu^{3+})4f	14.54 0.63	15.17	s(94.57%)p(0.03%)d(0.53%)f(4.85%) s(4.39%)p(0.15%)d(15.02%)f(80.38%)
$AmL^6(NO_3)_3$	LP(N/O)→LP*(Am^{3+})7s LP(N/O)→LP*(Am^{3+})5f	16.04 1.21	17.25	s(99.53%)p(0.06%)d(0.32%)f(0.09%) s(0.00%)p(0.07%)d(6.31%)f(93.61%)
$EuL^6(NO_3)_3$	LP(N/O)→LP*(Eu^{3+})6s LP(N/O)→LP*(Eu^{3+})4f	14.69 0.34	15.03	s(99.22%)p(0.05%)d(0.32%)f(0.38%) s(0.22%)p(0.06%)d(29.23%)f(70.41%)
$AmL^7(NO_3)_3$	LP(N/O)→LP*(Am^{3+})7s LP(N/O)→LP*(Am^{3+})5f	16.41 1.76	18.17	s(98.80%)p(0.06%)d(0.31%)f(0.83%) s(0.54%)p(0.36%)d(9.15%)f(89.95%)
$EuL^7(NO_3)_3$	LP(N/O)→LP*(Eu^{3+})6s LP(N/O)→LP*(Eu^{3+})4f	14.63 0.27	14.90	s(99.31%)p(0.06%)d(0.34%)f(0.27%) s(0.14%)p(0.03%)d(28.26%)f(71.50%)
$AmL^8(NO_3)_3$	LP(N/O)→LP*(Am^{3+})7s LP(N/O)→LP*(Am^{3+})5f	15.25 1.24	16.49	s(99.33%)p(0.06%)d(0.52%)f(0.09%) s(0.01%)p(0.06%)d(5.81%)f(94.12%)
$EuL^8(NO_3)_3$	LP(N/O)→LP*(Eu^{3+})6s LP(N/O)→LP*(Eu^{3+})4f	13.67 0.31	13.98	s(99.47%)p(0.06%)d(0.41%)f(0.04%) s(0.00%)p(0.05%)d(14.04%)f(85.89%)
$AmL^9(NO_3)_3$	LP(N/O)→LP*(Am^{3+})7s LP(N/O)→LP*(Am^{3+})5f	15.72 1.12	16.84	s(97.94%)p(0.06%)d(0.43%)f(1.57%) s(1.23%)p(0.39%)d(5.49%)f(92.90%)
$EuL^9(NO_3)_3$	LP(N/O)→LP*(Eu^{3+})6s LP(N/O)→LP*(Eu^{3+})4f	13.57 0.31	13.88	s(99.30%)p(0.05%)d(0.50%)f(0.13%) s(0.09%)p(0.03%)d(10.98%)f(88.87%)
$AmL^{10}(NO_3)_3$	LP(N/O)→LP*(Am^{3+})7s LP(N/O)→LP*(Am^{3+})5f	15.98 1.55	17.53	s(98.96%)p(0.06%)d(0.32%)f(0.66%) s(0.42%)p(0.34%)d(7.57%)f(91.67%)
$EuL^{10}(NO_3)_3$	LP(N/O)→LP*(Eu^{3+})6s LP(N/O)→LP*(Eu^{3+})4f	14.12 0.87	14.99	s(98.54%)p(0.07%)d (0.19%)f(1.19%) s(0.95%)p(0.17%)d(10.44%)f(88.38%)

Firstly, the total second-order stabilization energy in the Am(III) complexes is in the range of 15–19 kcal/mol, which is significantly greater than that in the corresponding Eu(III) complexes. Secondly, the 5f components in the acceptor NBO of the Am(III) interacting with the ligand are much larger than the 4f

DOI: 10.1063/1674-0068/cjcp2412162

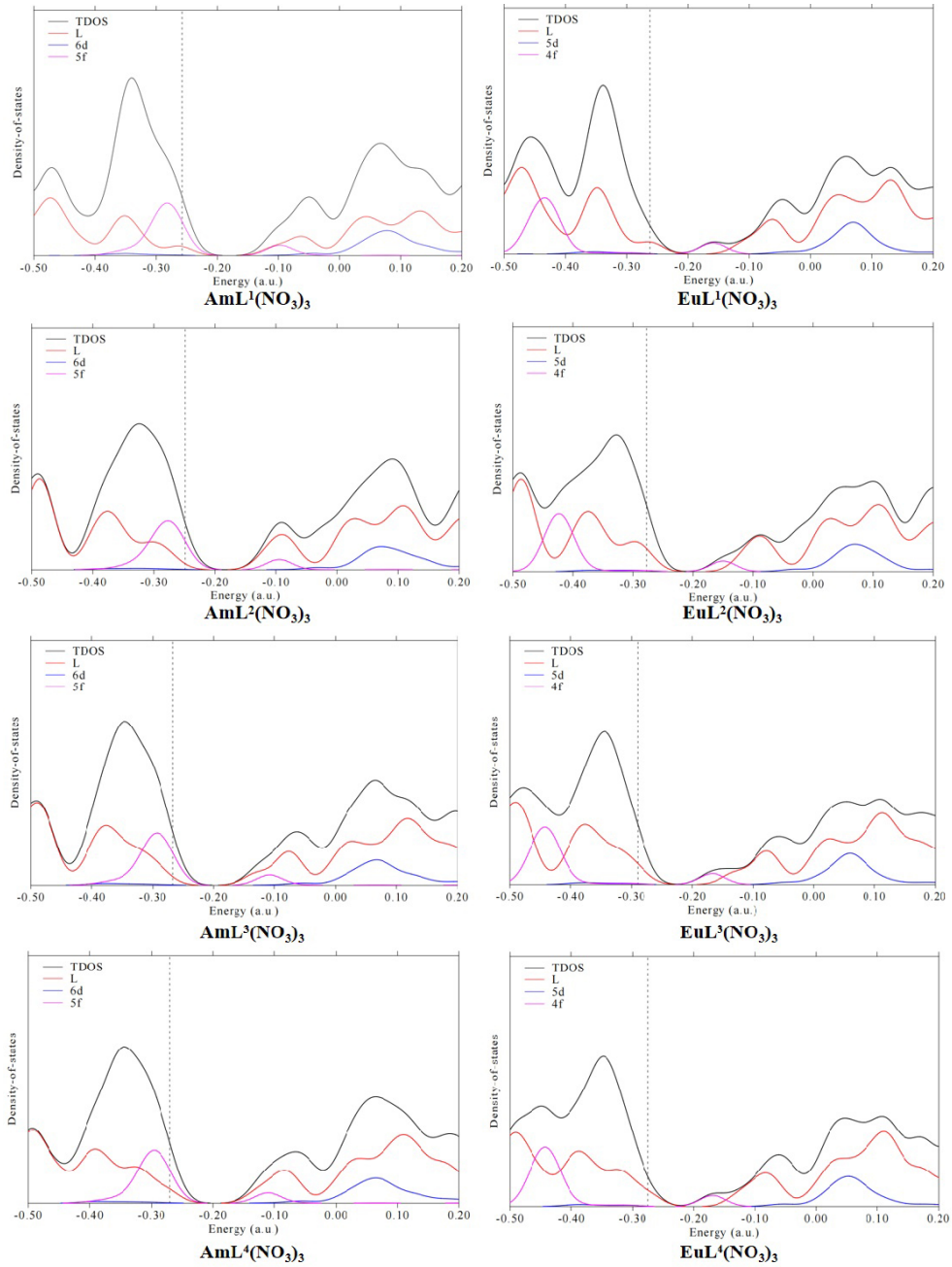

FIG. 5 TDOS and PDOS figures of the $ML(NO_3)_3$ complexes formed by symmetric ligands at the PBE0/6-311G(d)-RECP level of theory.

components contained in the Eu(III) acceptor NBO, thus the Am-5f orbitals are more involved in the interaction with the N/O lone pair orbitals than the Eu-4f orbitals, which is the fundamental reason why Am(III) has a stronger bonding ability than Eu(III). Finally, regarding the impact on the donor-acceptor hyperconjugation interaction, there is no obvious trend for symmetric or asymmetric ligands, and the ligands L^1, L^4, and L^7 have relatively large second-order stabilization energies.

The bonding characteristics of the metal ions Am(III) and Eu(III) with the ligands were further investigated by means of the density of states analysis (DOS). The total density of states (TDOS) and the three PDOS (partial density of states) of the ligand orbitals and the (n–2)f orbitals and (n–1)d orbitals of the metals were calculated at the PBE0/6-311G(d)-RECP level of theory, the DOS curves within the range from –0.50 a.u. to 0.20 a.u. are shown in FIG. 5 and FIG. S1 (SM) for the symmetric ligands and asymmetric lig-

DOI: 10.1063/1674-0068/cjcp2412162

ands, respectively. In the figures, the dotted line indicates the energy position of the HOMO. It can be seen from the figures that in most energy ranges, the PDOS curve of the ligand almost coincides with the TDOS curve, which indicates that the ligand orbitals contribute a significant proportion within these energy ranges. The TDOS and the PDOS curves of the (n–2)f orbitals and (n–1)d orbitals and the ligand orbitals show peaks simultaneously within approximately the same energy range for all ligands, which indicates that the differences in ligands have a relatively small impact on the density of states. When comparing the differences between $AmL(NO_3)_3$ and $EuL(NO_3)_3$, the Am-6d and Eu-5d PDOS curves exhibit approximately the same shape and both have a peak near the energy of 0.10 a.u.; while the PDOS curves of Am-5f and Eu-4f orbitals show significant differences, the Am-5f PDOS curve exhibits a peak within the energy range from –0.30 a.u. to –0.25 a.u., near the HOMO energy, however the Eu-4f PDOS curve shows a peak within the energy range from –0.45 a.u. to –0.40 a.u., far away from the HOMO energy. This means that the Eu-4f orbitals are more contracted than the Am-5f orbitals and are located in a lower energy range. Therefore, the Am-5f orbitals are more diffuse and are more involved in bonding with the ligands than the Eu-4f orbitals. This indicates that these ligands may be feasible for separating Am^{3+} and Eu^{3+}.

Thermodynamic analysis can be used to explore the extraction ability and separation performance of the ligands for the metal ions Am(III)/Eu(III). The extraction process was considered to be performed between the organic phase of the organic solvents n-dodecane or cyclohexanone and the aqueous phase. The CPCM solvation model was adopted to treat the solvation effect. The initial reactant was assumed to be the hydrated ion $Am(H_2O)_9{}^{3+}$ and the extraction product to be the 1:1 neutral complex $ML(NO_3)_3$. The extraction reactions are as follows:

$$\mathrm{Am\,(H_2O)_9{}^{3+}(aq) + L(org) + 3NO_3{}^{-}(aq) \rightarrow AmL\,(NO_3)_3\,(org) + 9H_2O^{-}(aq)}$$

$$\mathrm{Eu\,(H_2O)_9{}^{3+}(aq) + L(org) + 3NO_3{}^{-}(aq) \rightarrow EuL\,(NO_3)_3\,(org) + 9H_2O^{-}(aq)}$$

The Gibbs energy (ΔG_{ext}) of the extraction reactions was calculated by means of the PBE0/6-311G(d)-RECP method, which can be used to measure the extraction capacity of the ligands for the Am(III)/Eu(III) ions. The extraction selectivity and separation effect of the ligand for the two metals can be measured by means of the $\Delta\Delta G_{Am/Eu} = \Delta G_{ext}(Am) - \Delta G_{ext}(Eu)$ and the separation factor $SF_{Am/Eu}$ which is defined by the formula $\Delta\Delta G_{Am/Eu} = -RT\ln SF_{Am/Eu}$, where R is the gas constant and T is the temperature (298 K). All the results are listed in Table VI.

It can be seen from Table VI that the ΔG_{ext} of all the ligands are large negative values in both n-dodecane and cyclohexanone solvent environments, and there is no significant difference in the values of ΔG_{ext} for the two solvent phases, which indicates that the two-phase extraction reactions between the four ligands and Am(III)/Eu(III) can proceed automatically, and these ligands have good extraction ability for the two metal ions. The ΔG_{ext} in the cyclohexanone environment is more negative than that in the n-dodecane environment by 0.92–15.67 kcal/mol. Thus, the polar solvent environment of cyclohexanone is more favorable to the extraction of the metal ions than the non-polar environment of n-dodecane. In a given solvent environment and for a given metal ion the ΔG_{ext} of all the 10 ligands are very close to one another, distributed in a narrow range, which indicates that these ligands have very close extraction capabilities.

When comparing the two metal ions, Am(III) and Eu(III), in a given solvent environment, for each ligand, the $\Delta G_{ext}(Am)$ is always more negative than the corresponding $\Delta G_{ext}(Eu)$, and the $\Delta\Delta G_{ext}$ is always negative, in the range from −0.89 kcal/mol to −9.01 kcal/mol, which means that Am(III) can form stronger bond with these ligands than Eu(III), and these ligands have good extraction selectivity and separation performance for the two metal ions. Despite the obvious influence of solvent environment on separation factors, in both solvent environments, ligand L^9 has the best separation performance, ligand L^5 and L^8 also have good separation performance, while ligand L^6 has the smallest separation factor, and the separation effect of ligand L^4 is not ideal. The separation effect of other ligands in the two solvent environments is quite different, such as L^1, L^2, L^3 and L^7. The ligands L^9, L^5, L^8 and L^1 have better separation performance in the n-dodecane solvent, while ligands L^2, L^3, L^7 and L^{10} have larger separation factor in the cyclohexanone solvent. The asymmetric ligands L^9, L^5 and L^8 have better separation effect than the symmetric ligands. The distribution of N atoms on the side

DOI: 10.1063/1674-0068/cjcp2412162

TABLE VI The Gibbs energy of the extraction reactions (ΔG_{ext}, in kcal/mol) of the solvent extraction process for Am(III) and Eu(III) from the aqueous phase to the organic solution (cyclohexanone and n-dodecane) under acidic conditions calculated at the PBE0/6-311G(d)-RECP level of theory, the difference ($\Delta\Delta G_{Am/Eu}$ in kcal/mol) of ΔG_{ext} between Am(III) and Eu(III) and the separation factor ($SF_{Am/Eu}$).

Ligand	Cyclohexanone				*n*-Dodecane			
	ΔG_{ext}(Am)	ΔG_{ext}(Eu)	$\Delta\Delta G_{Am/Eu}$	$SF_{Am/Eu}$	ΔG_{ext}(Am)	ΔG_{ext}(Eu)	$\Delta\Delta G_{Am/Eu}$	$SF_{Am/Eu}$
L^1	−723.80	−720.91	−2.89	130.65	−714.77	−708.79	−5.98	23915.45
L^2	−721.31	−716.56	−4.75	3006.40	−705.55	−703.05	−2.50	67.69
L^3	−723.50	−719.14	−4.36	1557.69	−707.82	−704.91	−2.91	135.13
L^4	−720.15	−717.41	−2.74	101.46	−709.06	−706.24	−2.82	116.11
L^5	−722.85	−717.38	−5.47	10121.53	−718.32	−710.08	−8.24	1080181.89
L^6	−721.38	−720.49	−0.89	4.48	−715.57	−714.49	−1.07	6.07
L^7	−720.69	−715.05	−5.64	13481.05	−716.38	−714.97	−1.41	10.78
L^8	−721.72	−716.28	−5.44	9622.31	−716.02	−708.31	−7.71	441997.72
L^9	−722.53	−715.64	−6.89	110917.28	−716.09	−707.09	−9.01	3956159.03
L^{10}	−720.34	−716.25	−4.09	988.06	−713.25	−709.95	−3.30	260.81

chains has no obvious regularity on extraction selectivity and separation effect.

IV. CONCLUSION

In this work, we investigated the bonding properties as well as the extraction and separation characteristics of the N,O-hybrid ligands formed with furan as the skeleton with the Am(III)/Eu(III) ions in high-level liquid waste (HLLW). Ten symmetric and asymmetric ligands were constructed from the furan skeleton and the side chains of pyridine, pyridazine, pyrimidine and pyrazine, the ESP, the natural atomic charge, the HOMO and LUMO, and the protonation effect were calculated for these ligands. The coordination structures, bonding properties of the complexes $ML(NO_3)_3$ (M = Am, Eu) and the thermodynamics properties of the solvent extraction process of Am(III)/Eu(III) by the ligands were investigated using the PBE0/6-311G(d)-RECP method. The calculated results show that the M–O(furan) bond is significantly shorter than the M–N bond, while the WBI value of the former is smaller than that of the latter. The NBO and QTAIM analyses show that the bonds between Am(III)/Eu(III) and the ligands are typical closed-shell interaction and the Am-ligand bonds have some covalent character. The donor-acceptor interaction between the ligand and the metal ion causes a significant electron transfer from the ligand to the metal. The NBO analysis (second stabilization energy) and the DOS analysis demonstrate that the difference in the bonding properties of Am(III)/Eu(III) mainly stems from the fact that the Am-5f orbitals is more diffusive, more active, and more involved in bonding with the ligands than the Eu-4f orbitals, which confirms that the selectivity of the ligand for Am(III) is higher than that for Eu(III). The thermodynamics analysis shows that these ligands have strong extraction ability for the Am(III) and Eu(III) ions, and also have good extraction selectivity and separation performance for the two metal ions. The asymmetric ligand L^9 has the strongest separation performance for the Am(III) and Eu(III) ions, and the asymmetric ligands L^5 and L^8 also have good separation effect, the four symmetric ligands L^1, L^2, L^3, L^4 show moderate separation capacity, while the asymmetric ligand L^6 show the worst separation capacity. The distribution of N atoms on the side chains has an effect on extraction capacity and separation effect, but there is no obvious regularity. This research is helpful for understanding the flexible furan structural pattern on the actinide/lanthanide selectivity and can provide a suitable structural reference and valuable information for designing efficient extractants for the separation of Am(III)/Eu(III) from high-level liquid waste.

Supplementary materials: The average natural charges and bond lengths in different solvents, QTAIM analysis data for bond-related insights, TDOS and PDOS figures to show electronic density, and the optimized molecular coordinates for further exploration are shown.

DOI: 10.1063/1674-0068/cjcp2412162

[1] J. M. Mckibben, Radiochim. Acta **36**, 3 (1984).
[2] Y. D. Zhang, R. Su, X. F. Chen, C. Ren, Y. J. Lv, D. Mo, M. Liu, and S. J. Yan, J. Radioanal. Nucl. Chem. **322**, 1657 (2019).
[3] Y. Y. Zhang, S. Q. Wu, and A. Y. Li, New J. Chem. **46**, 14532 (2022).
[4] M. J. Hudson, L. M. Harwood, D. M. Laventine, and F. W. Lewis, Inorg. Chem. **52**, 3414 (2013).
[5] Z. P. Wang, S. D. Ding, X. Y. Hu, S. M. Li, D. P. Su, L. R. Zhang, Y. Liu, and Y. D. Jin, Sep. Purif. Technol. **181**, 148 (2017).
[6] H. H. Dam, D. N. Reinhoudt, and W. Verboom, Chem. Soc. Rev. **36**, 367 (2007).
[7] T. V. Malinina, V. I. Murina, L. N. Medvedeva, D. Y. Yakovlev, and E. S. Yushkov, At. Energy **126**, 59 (2019).
[8] R. Natarajan, Prog. Nucl. Energy **101**, 118 (2017).
[9] N. Bessen, Q. Yan, N. Pu, J. Chen, C. Xu, and J. Shafer, Inorg. Chem. Front. **8**, 4177 (2021).
[10] X. X. Wang, J. X. Li, S. Y. Dai, T. Hayat, A. Alsaedi, and X. K. Wang, Chem. Eng. J. **273**, 588 (2015).
[11] H. L. Zhang, A. Li, K. Li, Z. P. Wang, X. C. Xu, Y. X. Wang, M. V. Sheridan, H. S. Hu, C. Xu, E. V. Alekseev, Z. Y. Zhang, P. Yan, K. C. Cao, Z. F. Chai, T. E. Albrecht-Schönzart, and S. A. Wang, Nature **616**, 482 (2023).
[12] M. A. Denecke, A. Rossberg, P. J. Panak, M. Weigl, B. Schimmelpfennig, and A. Geist, Inorg. Chem. **44**, 8418 (2005).
[13] Z. Kolarik, U. Müllich, and F. Gassner, Solvent Extr. Ion Exch. **17**, 23 (1999).
[14] C. Ebenezer and R. V. Solomon, Comments Inorg. Chem. **44**, 385 (2024).
[15] Y. C. Hou, J. Wang, Y. R. Guo, S. D. Ding, and Q. J. Pan, Chem. Eng. J. **485**, 150138 (2024).
[16] X. Y. Zhang, L. L. Ye, W. H. Chen, X. F. Zhang, W. W. Chen, M. G. Chen, and P. W. Huang, ACS Omega **9**, 12060 (2024).
[17] E. Aneheim, C. Ekberg, A. Fermvik, M. R. S. J. Foreman, B. Grűner, Z. Hájková, and M. Kvičalová, Solvent Extr. Ion Exch. **29**, 157 (2011).
[18] C. Ekberg, E. Löfström-Engdahl, E. Aneheim, M. R. S. Foreman, A. Geist, D. Lundberg, M. Denecke, and I. Persson, Dalton Trans. **44**, 18395 (2015).
[19] A. Bremer, C. M. Ruff, D. Girnt, U. Müllich, J. Rothe, P. W. Roesky, P. J. Panak, A. Karpov, T. J. J. Müller, M. A. Denecke, and A. Geist, Inorg. Chem. **51**, 5199 (2012).
[20] G. Benay and G. Wipff, J. Phys. Chem. B **117**, 1110 (2013).
[21] S. Q. Wu, Y. Y. Zhang, and A. Y. Li, ChemistrySelect **7**, e202203622 (2022).
[22] V. S. Bryantsev and B. P. Hay, Dalton Trans. **44**, 7935 (2015).
[23] M. J. Frisch, G. W. Trucks, H. B. Schlegel, G. E. Scuseria, M. A. Robb, J. R. Cheeseman, G. Scalmani, V. Barone, B. Mennucci, G. A. Petersson, H. Nakatsuji, M. Caricato, X. Li, H. P. Hratchian, A. F. Izmaylov, J. Bloino, G. Zheng, J. L. Sonnenberg, M. Hada, M. Ehara, K. Toyota, R. Fukuda, J. Hasegawa, M. Ishida, T. Nakajima, Y. Honda, O. Kitao, H. Nakai, T. Vreven, J. A. Montgomery, Jr. , J. E. Peralta, F. Ogliaro, M. Bearpark, J. J. Heyd, E. Brothers, K. N. Kudin, V. N. Staroverov, R. Kobayashi, J. Normand, K. Raghavachari, A. Rendell, J. C. Burant, S. S. Iyengar, J. Tomasi, M. Cossi, N. Rega, J. M. Millam, M. Klene, J. E. Knox, J. B. Cross, V. Bakken, C. Adamo, J. Jaramillo, R. Gomperts, R. E. Stratmann, O. Yazyev, A. J. Austin, R. Cammi, C. Pomelli, J. W. Ochterski, R. L. Martin, K. Morokuma, V. G. Zakrzewski, G. A. Voth, P. Salvador, J. J. Dannenberg, S. Dapprich, A. D. Daniels, F. J. B. Farkas, J. V. Ortiz, J. Cioslowski, and D. J. Fox, *Gaussian 09 Revision D. 1*, Wallingford: Gaussian Inc, (2009).
[24] A. Klamt and G. Schüürmann, J. Chem. Soc. Perkin Trans. **2**, 799 (1993).
[25] A. Klamt, V. Jonas, T. Bürger, and J. C. W. Lohrenz, J. Phys. Chem. A **102**, 5074 (1998).
[26] M. Kaneko, H. Suzuki, and T. Matsumura, Inorg. Chem. **57**, 14513 (2018).
[27] S. Q. Wu and A. Y. Li, Phys. Chem. Chem. Phys. **26**, 1190 (2024).
[28] X. Y. Cao and M. Dolg, J. Mol. Struct. THEOCHEM **581**, 139 (2002).
[29] X. Y. Cao and M. Dolg, J. Mol. Struct. THEOCHEM **673**, 203 (2004).
[30] T. Lu and F. W. Chen, J. Comput. Chem. **33**, 580 (2012).
[31] A. E. Reed and F. Weinhold, J. Chem. Phys. **78**, 4066 (1983).
[32] A. E. Reed, R. B. Weinstock, and F. Weinhold, J. Chem. Phys. **83**, 735 (1985).
[33] W. Humphrey, A. Dalke, and K. Schulten, J. Mol. Graphics **14**, 33 (1996).
[34] X. F. Yang, Y. Liu, W. Q. Tao, S. Wang, P. Ren, S. L. Yang, L. Y. Yuan, H. B. Tang, Z. F. Chai, and W. Q. Shi, J. Environ. Chem. Eng. **10**, 108401 (2022).
[35] I. Fryer-Kanssen, J. Austin, and A. Kerridge, Inorg. Chem. **55**, 10034 (2016).

DOI: 10.1063/1674-0068/cjcp2412162